THE EFFECT OF PROCESS PARAMETERS IN EXTRUDING SCAFFOLD DESIGN USING SYNTHETIC BIOMATERIALS

Mohd Khairol Anuar Mohd Ariffin[1], Nor Aiman Sukindar[2], B T Hang Tuah Bin Baharudin[1], Che Nor Aiza Binti Jaafar[1], Mohd Idris Shah Bin Ismail[1]

[1]Department of Mechanical and Manufacturing, Universiti Putra Malaysia, 43300 Serdang, Malaysia
[2]Department of Manufacturing and Materials Engineering; Kuliyyah of Engineering, International Islamic University Malaysia, 50728 Kuala Lumpur, Malaysia

Corresponding author: Mohd Khairol Anuar Mohd Ariffin, khairol@upm.edu.my

Abstract: Open-source 3D printers have become a popular technology for inexpensively and rapidly fabricating three-dimensional products, including those for medical use. We developed and tested a nozzle for extruding synthetic biomaterials for fabricating scaffold structures that can be used as a medium for cell growth in, for instance, orthopedic replacements. The nozzle was designed iteratively to optimise the die angle, nozzle diameter, and liquefier shape for extruding bioresorbable polymers, and a thermal insulator was installed to maintain consistent temperature in the liquefier chamber. We then fabricated a range of scaffold structure parts with varying percentages of infill material and infill patterns. Analysis of variance tests show that the percentage of infill is a dominant factor affecting the porosity as well as the mechanical properties of the samples. Samples with 10%–30% of infill with a combination of lined infill patterns exhibited 50%–70% porosity with 12–20 MPa compressive strengths. These specifications are well-suited for cell growth. To demonstrate the feasibility of fabricating structures with consistent porosity with open-source printers, a humerus bone was 3D printed using both Polylactic acid (PLA) and polymethylmethacrylate (PMMA) filament, and the porosity was controllable. This study suggests that open-source 3D printers may be used for printing bone replacements in the near future.
Key words: Open-source 3D Printer, 3D Printer Nozzle, Synthetic biomaterial, Scaffold Design.

1. INTRODUCTION

Various fabrication techniques for rapid prototyping with synthetic biomaterials have been developed using conventional methods, including gas foaming, fiber bonding, membrane lamination, melt molding, particulate leaching, and solvent casting (Hutmacher, 2000). Another technique using polymeric sponge in the preparation of hydroxyapatite (HA) slurry for the fabrication of porous structure was reported (Monmaturapoj and Yatongchai, 2011). Scalera et al. (2013) also fabricated scaffold structure by using sponge replica method with the treatment of calcination. These techniques, however, struggle to fabricate scaffold structures, often failing to produce completely interconnected pores, limiting the practically useful technologies for fabricating orthopedic replacements only to those capable of building a scaffold design consistently and uniformly (Zein et al., 2002). The introduction of rapid prototyping (RP) technology has had a significant impact on artificial tissue engineering. Also known as free form fabrication or additive manufacturing, RP includes a range of techniques. Among these, stereolithography, inkjet printing, color jet printing, selective laser sintering, and fused deposition modeling (FDM)[1] are the most popular techniques due to their ability in extruding plastics (Chen et al., 2007). FDM is a popular technique for fabricating scaffold designs due its flexibility in controlling pore size as well as its ability to fabricate complex three-dimensional (3D) structures. Zein et al. (2002) used FDM method to fabricate porous structure with honeycomb-like pattern using bioresorbable polymer poly (ε-caprolactone) (PCL). The same method was used by Espalin et al. (2010) in fabricating the porous structure using different material which was polymethylmethacrylate (PMMA). Park et al. (2012) fabricated porous structure using two different materials which were PCL and poly (d,l-lactic-glycolic acid) (PLGA) and showed that PLGA degraded much faster than PCL. The use of PCL is preferable due to slow degradation especially when treating critical defects. A study on polymer–ceramic composite was also done by mixing polypropylene (PP) polymer and tricalcium phosphate (TCP) ceramic (Kalita et al., 2003). The results showed that this material was suitable for fabrication of scaffold structure which possessed non-toxic characteristic and exhibited excellent growth. A similar study was performed on the composite using PCL/hydroxyapatite (PCL/HA) with 25% concentration by weight of HA and the outcome showed that HA affected the mechanical properties of scaffold structure (Shor et al., 2010). Despite being the

[1] Trademark Stratasys, Inc

popular technology in fabricating scaffold structure, most commercially available FDM technologies involve high-cost machines, making the technology only available to well-funded institutions or organizations.

The era of open-source 3D printing began after the recent expiration of patents on FDM technology. Despite the growing market for 3D model fabrication, the cost of quality 3D printing machines is beyond the reach of most consumers. Many researchers have tried to reduce the cost of 3D printers, for example Adrian Bowyer and his team invented a low-cost 3D printer in the mid-2000s (Richardson, 2012). This 3D printer is known as the Replicating Rapid Prototyper (RepRap), and it was designed to be reproduced using open-source plans and easily accessible tools (Jones et al., 2011). Since then, commercial models have been developed based on RepRap projects such as RepRap Mendel Prusa, Makerbot Industries Cupcake, and Ultimaker (Richardson, 2012).

The 3D printing process begins with a filament pushed into a liquefier chamber via a motor in which the temperature is monitored by a thermocouple. The semimolten polymer is then extruded by the force of the motor and is deposited layer by layer. A new layer is laid on the top of the recently solidified layer. This process is repeated until the part is finished. Figure 1 illustrates this 3D printing process.

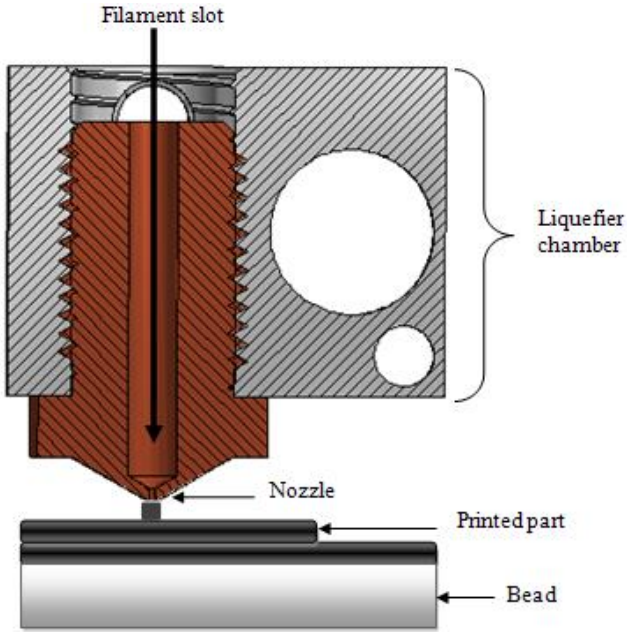

Fig. 1. Diagram of 3D-printing extrusion process

Figure 2 shows the process parameters involved in printing. Each parameter can be controlled via inputs into the slicing software. Every layer is deposited according to the slice height (SH), which can be set at 0.2mm or larger with 0.1mm increment, depending on the desired surface finish. The width of the deposited layer is called the road width (RW) and it can be controlled by varying the printing speed and nozzle-tip diameter. The print head of the 3D printer forms raster angles by moving in the x and y directions and manipulates the build orientation transversally or axially by moving in the z direction. The air gap (AG), which is the distance between each layer, affects the mechanical properties of the printed material and is set to 0 by default (Onwubolu and Rayegani, 2014). All the process parameters involved need to be carefully observed to have desired product finishing especially to those related to the application in medical field.

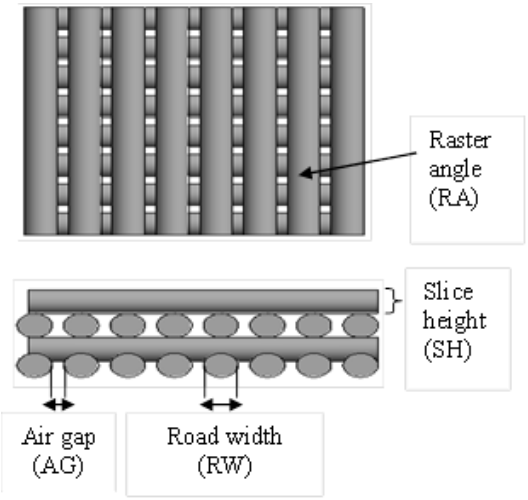

Fig. 2. Parameters setting for 3D printing

The importance of 3D printing application in medical field has recently increased. Novel synthetic biomaterials present great opportunities for manufacturing orthopedic replacements. A process to simulate natural extracellular matrices (ECMs) that uses rapidly fabricated 3D extracellular microenvironments has been developed (Lutolf and Hubbell, 2005). Synthetic biomaterials can be used for fabricating ECMs because of their biodegradability characteristic. This allows for a synthetic skeleton to be replaced with living cells and connected seamlessly with living tissue. Polylactic acid (PLA) and polymethylmethacrylate (PMMA) are the most popular polymers used for such medical applications. PLA is commonly used in sutures and tissue engineering (Binnaz Hazar Yoruc and Cem Sener, 2015). Meanwhile PMMA is used for different medical applications such as bone cement and dentures (Nair and Laurencin, 2006).

To print effectively with synthetic biomaterials, the flow behavior of the material inside the nozzle needs to be optimized. Issues related to stability, consistency, and accuracy have been reviewed where different materials have different convergent angles which affect the flow behavior along the liquefier (Liang and Ness, 1997). Nozzle diameter also affects the pressure

drop which influences the flow material (N.A. Sukindar et al., 2016). Another study related to pressure drop along the liquefier by manipulating the die angle as well as nozzle diameter was also reported (Ramanath et al., 2008). The findings showed that when the nozzle angle became larger, the pressure drop decreased and larger nozzle diameter contributed to lower pressure drop. The nozzle design is a key for a successful extruding of synthetic biomaterials. The present study investigates the ability of an open-source 3D printer to fabricate bioresorbable scaffolds with fully interconnected channel networks. We modified the nozzle of a common open-source 3D printer for use with synthetic biomaterials. Our modifications yielded a nozzle that can extrude parts with porosities in the range needed for ECMs.

2. MATERIALS AND METHODS

2.1 3D Printer Optimization

A variation on open-source 3D printers was designed to investigate low-cost biomedical printing. It is powered by five stepper motors with three degrees of freedom, in the x, y, and z directions, as shown in Figure 3. The printing head was moved through each axis by a lead screw, which is more precise than driving the mechanism with belting. The software controller uses the Repeater Host software, which communicates between the host computer and microcontroller serially. Both the hardware and software systems of the 3D printer must be customized to effectively extrude the PLA and PMMA materials. This study focuses on developing a novel nozzle and tuned the process parameters in the 3D printer software.

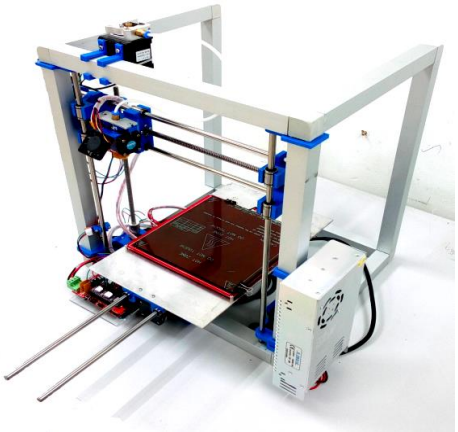

Fig. 3. Open-source 3D-printer

2.2 Nozzle fabrication

The 3D printer nozzle is a core component in determining the success of an extrusion process. Several factors affect the stability, accuracy, and consistency of 3D printing. These factors include the die angle, which affects the stability and consistency of a scaffold design. When the molten material flows onto the die angle, this flow may cause shear and lead to a pressure drop along the liquefier. To reduce this effect, the angle of the molten material flow, which is known as natural convergent angle, must be close to the die angle of the nozzle. Previous studies suggested that if the natural convergent angle is close to the die angle, the stability and consistency of the extrusion process can be improved (Liang and Ness, 1997). The liquefier chamber must be designed according to the material being extruded. The dynamic environment inside the liquefier introduces the challenges of ensuring that the material has sufficient room to expand as it melts and maintaining constant viscosity. If the viscosity changes constantly, the flow rate changes, causing instability in the extrusion process (Bellini and Guceri, 2003). We chose a cylindrical liquefier design, which provided better heat transfer than that of the standard nozzle. When determining the RW of the scaffold to be printed, the nozzle-tip diameter needs to be selected carefully. It is shown that smaller diameter yields higher pressure drop, and the pressure drop significantly affects the RW of the scaffold design (Mostafa et al., 2009). However, a small nozzle diameter is essential it reduces geometrical errors (Brooks et al., 2012). Considering the efficiency of the extrusion process, however, smaller diameter nozzle leads to a longer printing process. With consideration of all these factors, we chose a 0.3 mm diameter nozzle tip for our nozzle prototype. Heat convection may also occur during the printing process; therefore, an insulator was fabricated for the nozzle to maintain a stable and constant temperature. Figure 4 shows the nozzle developed in this study.

2.3 Process optimisation

Extrusion in the FDM process depends mostly on the liquefier temperature and feed rate, which need to be carefully monitored (Espalin et al., 2010). The bead temperature also needs to be optimised to yield a properly adhered bead such that the parts do not shrink or warp. The printing temperature affects the printing of porous structures directly (Zein et al., 2002). To determine the optimum printing temperature, simple square prisms were fabricated with various liquefier temperatures ranging from 160°C to 260°C and the process was monitored. Low temperatures of 160°C to 180°C yield an unstable extrusion process, yielding brittle parts with very rough surfaces. High temperature of 260°C creates excessive material residue and the finished parts are expanded due to the high temperature. The temperature of 190°C was found to be the optimum temperature for PLA material, while PMMA material is best extruded at 200°C.These provide good RW and no sign of expansion. Bead temperatures were tested within the range from 45°C to 60°C.

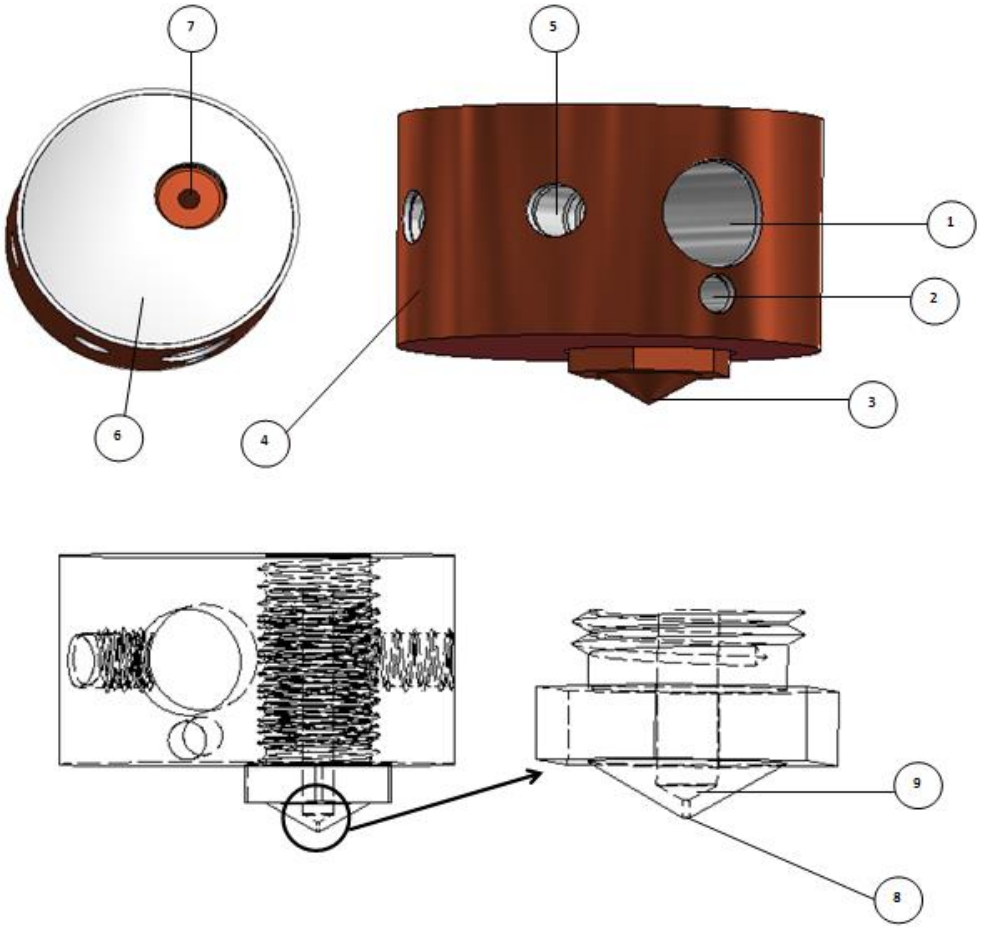

Fig. 4. Nozzle 3D renderings and schematics: 1-Heating slot; 2-Thermocouple slot; 3-Nozzle; 4-Insulator; 5-Screw slot; 6-Liquefier; 7-Nozzle slot; 8-Nozzle-tip diameter; 9-Die angle

The lower temperature of 45°C can cause the parts to warp as layers are not properly adhered to the bead. Meanwhile, a high temperature of 60°C causes the bottom layers to expand so the component is very difficult to remove after the parts is finished. A bead temperature of 50°C was found to be the optimum as there is no sign of warping or shrinkage and it provides enough adhesion to the bead. Some modifications were made to the bead by staging the part on tempered glass to allow easy removal of the finished parts. For open-source 3D printers, the printing speed can also be adjusted. The printing speed was varied from 20mm/s to 100mm/s. Printing speeds between 20mm/s and 50 mm/s yield uneven layer thicknesses and each layer becomes so thick that it affects the accuracy of the RW. Speeds between 80 mm/s to 100mm/s cause under-deposited layers such that the layers are too thin and the final part is smaller than intended. The optimum printing speed was 60mm/s, which yields consistent RW and consistent layer thickness of the finished parts.

2.4 Characterisation of scaffold design

The scaffold was designed with special attention to its mechanical properties and porosity. All the samples were subjected to compression tests that measured the yield strength and yield strain. The dimensions and weights of all samples were also measured to estimate the porosity of the scaffold design. The first experiment analysed the internal scaffold design's effect on the component's mechanical properties and the second experiment evaluated the effect of the infill pattern on the porosity and mechanical properties.

2.4.1 Sample preparation

PLA (Emlabz Technology Sdn Bhd, Kuala Lumpur, Malaysia) and PMMA (DR3D Filament Ltd., UK) materials were used in the form with of 1.75mm diameter filaments. For the experiment, samples of square prisms with dimensions 7×7×13.5mm were designed using Autodesk Inventor Software (Autodesk, USA), exported to STL format, and samples were printed with different infill percentages and infill patterns. This experiment evaluated the effect of the grid and line infill pattern on the mechanical properties and porosities of printed parts. The 0.3-mm-diameter nozzle tip was used to fabricate the fourty samples, of which twenty samples underwent compressive testing and twenty samples were used for observing the structure. These tests were performed with both the PLA and PMMA samples. All the details of the samples are recorded in Table 1.

Table 1. Sample specifications

Sample	Condition			
	Shell thickness (mm)	SH (mm)	Percentage infill (%)	Infill pattern
1	1	0.3	10	Grid / Line
2			20	
3			30	
4			40	
5			50	

2.4.2 Porosity

The porosity of the fabricated part was estimated according to the ASTMF 2450-04 standard. We followed the method in our previous research (Espalin et al., 2010) using the equation (1):

$$V_p = V_T - \frac{m_s}{\rho_s} \quad (1)$$

where V_T is the total scaffold volume, V_P is the total volume occupied by the porous network, m_s is the total sample mass, and ρ_s is the material density,which is 1.3g/cm^3 for PLA and 1.2g/cm^3 for PMMA. The porosity can be calculated using the equation (2):

$$\text{Porosity } (\%) = \frac{V_F}{V_T} \times 100 \quad (2)$$

2.5 Compressive testing

Compressive test were conducted for samples with both infill patterns using the Instron 3366 dual column table top universal testing system (Singapore) with the same method in previous studies(Espalin et al., 2010) based on the ASTM F451-08 standard. Compression tests were performed at a cross-head speed of 1mm/min and with a 10kN load cell. Compressive stress–strain curves were plotted.

2.6 Imaging

Twenty samples were observed with anoptical microscope (OptikaMicrocope PRO519 CU, Italy). We noted the scaffold structure and measured the dimensions to calculate porosities. The measurements were repeated five times for the sake of accuracy.

2.7 Statistical analysis

The minitab 16.0 software (Minitab, USA) was used for statistical analysis. For these tests, analysis of variance (ANOVA) was applied to compare the mean value of in dependent samples. *p*-values less than 0.05 were chosen to be significant.

3. RESULTS AND DISCUSSION

3.1 Porosities

All the sample structures were printed from both PLA and PMMA, as shown in Figure 6 and Figure 7. The porosity results for both PLA and PMMA samples are listed in Tables 2 and 3. The infill percentage was varied from 10% to 50% for the grid and line infill patterns. In Figure 5, the line pattern is pictured. Figure 6 pictures the grid infill pattern.

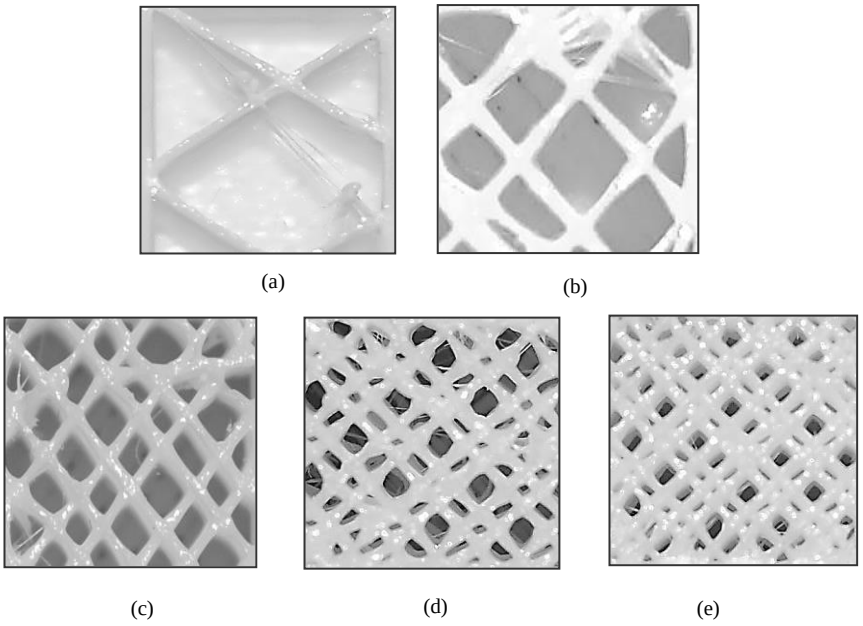

Fig. 5. Scaffold structure for PLA material with line infill pattern. (a) 10% infill (b) 20% infill (c) 30% infill (d) 40% infill (e) 50% infill

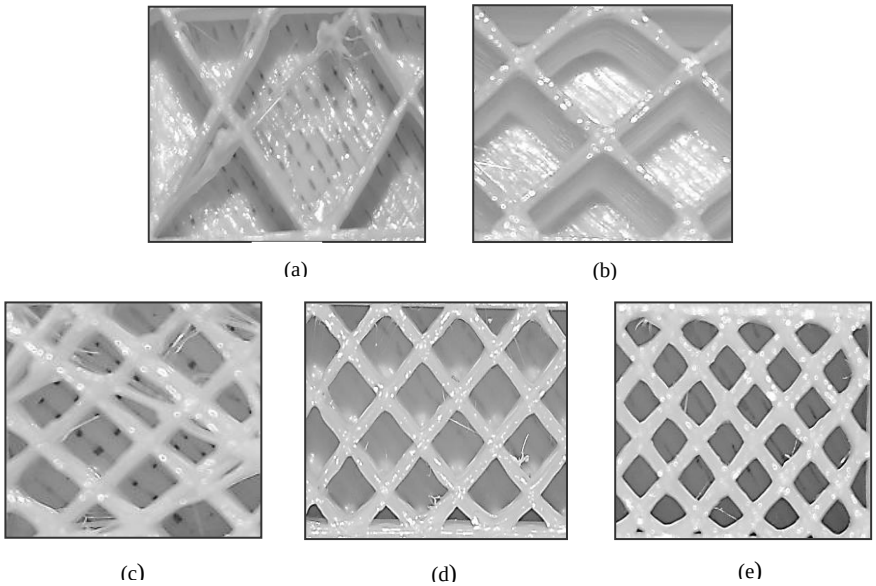

Fig. 6. Scaffold structure for PMMA material with grid infill. (a) 10% infill (b) 20% infill (c) 30% infill (d) 40% infill (e) 50% infill

Table 2. Sample porosities with line infill pattern

Sample	Infill percentage (%)	Infill pattern	Average mass (g)		Average V_T (mm^3)		Average V_P (mm^3)		Average Porosity (%)	
			PLA	PMMA	PLA	PMMA	PLA	PMMA	PLA	PMMA
1	10	Line	0.25	0.24	661.50	661.39	469.19	461.39	70.9	69.8
2	20		0.32	0.30	661.95	661.39	415.80	411.39	62.8	62.2
3	30		0.43	0.42	661.50	661.34	330.73	311.34	50.0	47.1
4	40		0.51	0.48	662.18	662.80	269.87	262.48	40.8	39.6
5	50		0.59	0.57	661.50	660.45	207.65	185.45	31.4	28.1

Table 3. Porosities samples for grid infill pattern

Sample	Infill percentage (%)	Infill pattern	Average mass (g)		Average V_T (mm^3)		Average V_P (mm^3)		Average Porosity (%)	
			PLA	PMMA	PLA	PMMA	PLA	PMMA	PLA	PMMA
1	10	Grid	0.22	0.21	662.45	663.39	493.22	488.39	74.5	73.6
2	20		0.29	0.28	661.95	661.39	438.87	428.10	66.3	64.7
3	30		0.39	0.37	661.50	661.34	361.50	353.00	54.6	53.4
4	40		0.48	0.46	663.39	662.45	294.16	279.12	44.3	42.13
5	50		0.55	0.53	662.45	663.39	239.37	221.72	36.13	33.4

Table 4. Analysis of variance for percentage of porosity

Material	Source	DF	SS	MS	F	P
PLA	A	4	2002.04	500.51	2580.08	0.000
	B	1	39.72	39.72	204.76	0.000
	Error	1	0.78	0.19		
	Total	9	2042.54			
PMMA	A	4	2192.05	548.01	384.77	0.000
	B	1	41.74	41.74	29.31	0.006
	Error	1	5.70	1.42		
	Total	9	2239.48			

ANOVA analysis showed that the porosity percentages were affected by the infill percentage (A)(p=0.000) for both materials PLA and PMMA as shown in Table 4. Higher infill percentage lends more solidity to the structure but the porosity was reduced. Infill pattern (B) also showed statistically significant effect (p=0.000) for PLA and (p = 0.006) for PMMA. The infill percentage and infill pattern plays an important part in influencing the porosity percentage, as shown in Figure 7.

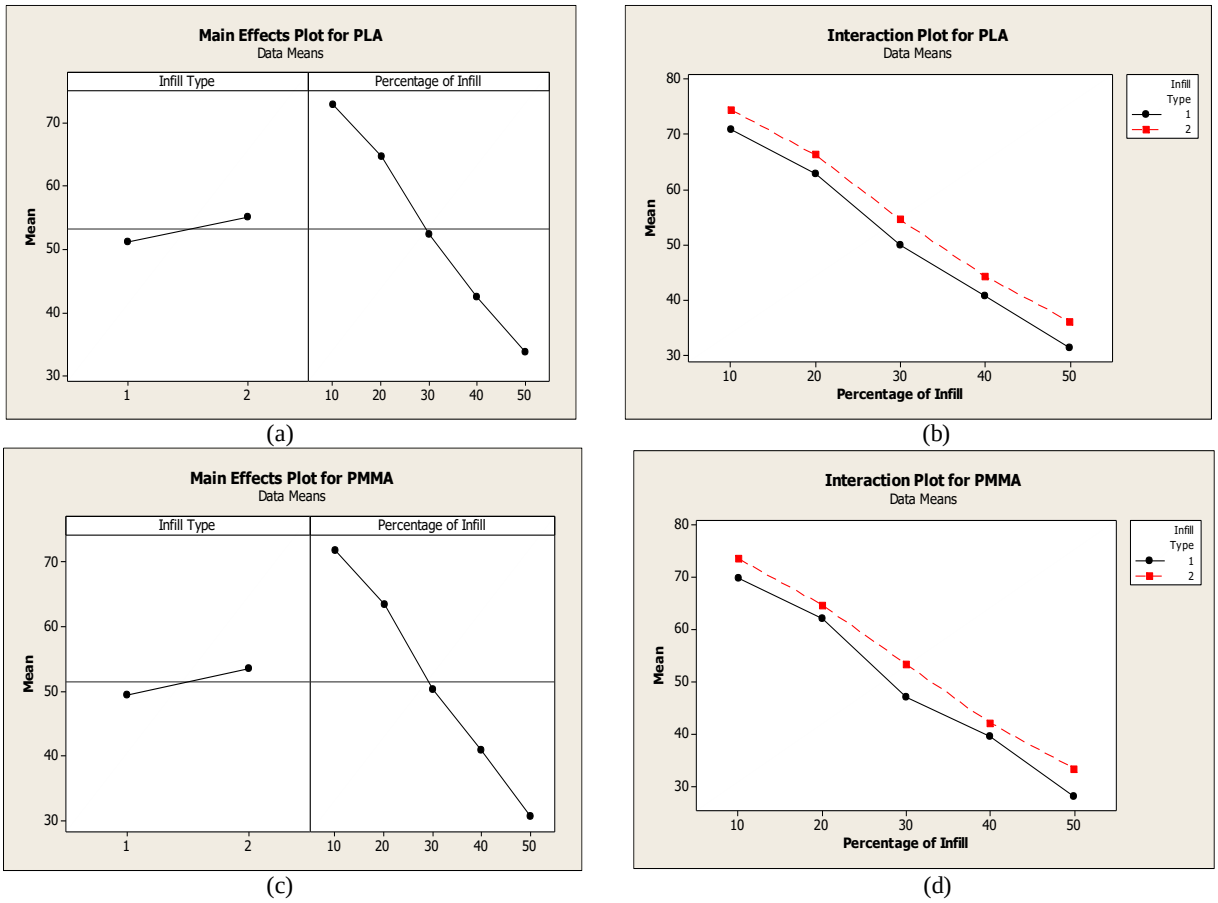

Fig. 7. Main effects and interaction plot for porosities. (a) Effect infill pattern and infill percentage for PLA; (b) Interaction of infill percentage and infill pattern for PLA; (c) Effect infill pattern and infill percentage for PMMA; (d) Interaction of infill percentage and infill pattern for PMMA

Figure 7 shows that infill pattern (Type 1: Line, Type 2: Grid) and infill percentage does affect the percentage of porosity. Turning to the interaction plot, infill percentage and infill pattern are positively correlated, with both affecting the porosity percentage. Regarding Figures 5 and 6, the grid infill pattern yields a more-porous structure than does the line infill pattern. Samples printed with a grid infill pattern were lighter in weight than those with a line infill pattern, which indicates the difference in porosities, as summarized in Tables 2 and 3. Sample 5 printed with both materials showed the lowest porosity, around 28% to 36%, while sample 1 showed the highest porosity, at approximately 70%. The range of 50%–70% porosity is the ideal for cell growth (Espalin et al., 2010b; Zein et al., 2002) and it was produced with samples 1, 2, and 3 as shown in Figure 8.

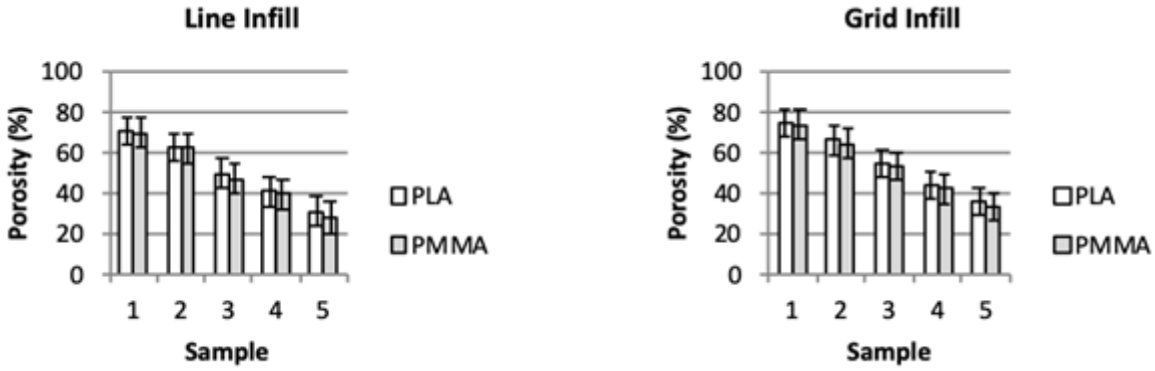

Fig. 8. Porosity percentage for PLA and PMMA printed parts

With an optical microscope (Optika Microcope PRO519 CU, Italy), the porous structure of the grid infill pattern for PLA and PMMA material can be seen clearly as shown in Figure 9.

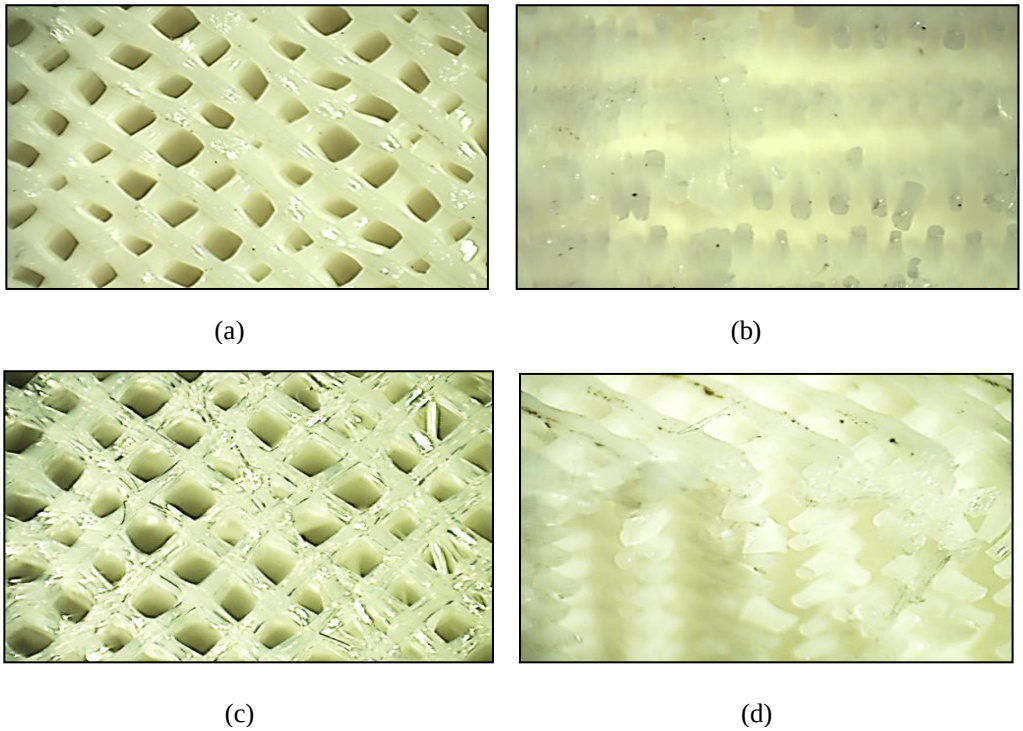

(a) (b)

(c) (d)

Fig. 9. The scaffold structure for grid infill PLA and PMMA prints (× 20 magnification). (a) Top view of PLA sample, (b) Side view of PLA sample, (c) Top view of PMMA sample, (d) Side view of PMMA sample

3.2 Mechanical properties

Compressive testing was performed on all samples and ANOVA results show that the infill percentage (A) and infill patterns (B) significantly affect the mechanical properties as shown in Table 5.

Table 5. Analysis of variance for mechanical properties

Material	Source	DF	SS	MS	F	P
PLA	A	4	195.647	48.912	326.08	0.000
	B	1	4.900	4.900	32.67	0.005
	Error	4	0.600	0.150		
	Total	9	201.147			
PMMA	A	4	187.235	46.809	485.95	0.000
	B	1	7.225	7.225	75.01	0.001
	Eroor	4	0.385	0.096		
	Total	9	194.846			

The *p*-value for infill percentage is p=0.000 for PLA and PMMA.Meanwhile, the *p*-value for infill pattern is p = 0.005 for PLA and for PMMA is p = 0.001, which is also statistically significant. Figure 10 shows the main-effect plot as well as interaction plots for both materials. The main-effect plot shows that sample 5 (infill percentage 50%) displayed a major effect on compressive strength. From the interaction plot, the line infill pattern provides higher compressive strength compared to the grid infill pattern. This fact can also be leveraged to optimize the porosity percentages.

Compressive stress–strain curves were plotted for all samples and the result shown in Figures 11. 50% infill with a line patterns, sample 5 provides higher compressive strength, around 20MPa, while 10% infill, sample 1 recorded the lowest compressive strength, around 7MPa, as shown in Figure 12. For grid infill patterns, sample 5 shows the highest compressive strength for 50% infill and sample 1 shows the lowest compressive strength for 10% infill. Our previous study showed that infill percentage affects tensile strength (Melenka et al., 2015). The present finding suggests that tensile strength can be increased by increasing the infill percentage. For fabricating a porous structure, the infill percentage must be chosen carefully. Lower compressive strength allows higher porosity, which is necessary for encouraging cell growth. Different parts bones have different compressive strengths and porosities, from 3MPa to 15MPa and 50% to 70%, respectively. For the trabecular bone, the ideal conditions for cell growth are structures with porosity in the range from 70% to 90% and compressive strength from 3MPa to 15MPa (Espalin et al., 2010). Samples 1, 2, and 3 meet those conditions printed with both infill patterns. This success shows that the 3D printer can fabricate porous scaffold structures out of common biomaterials.

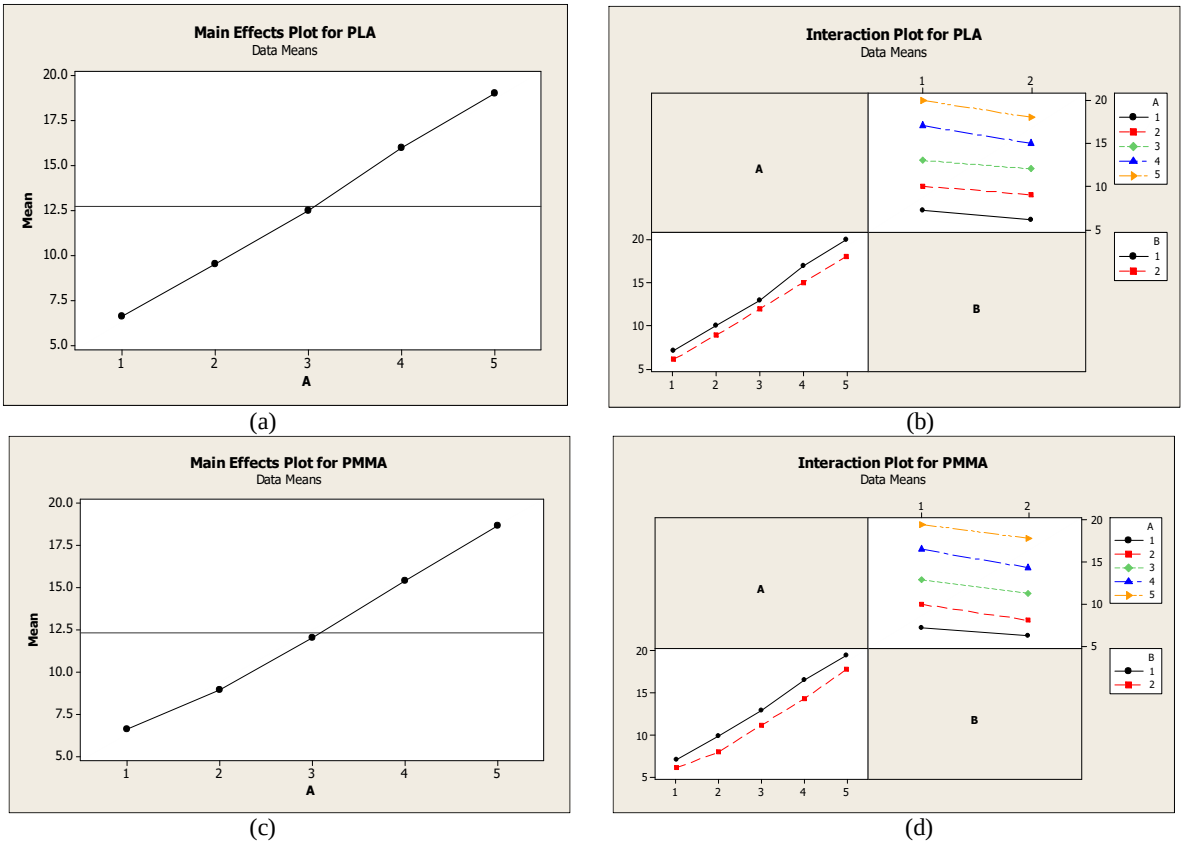

(a) (b)

(c) (d)

Fig. 10. Main-effect and interaction plots for compressive strength. (a) Effect of infill percentage for PLA (b) Interaction of infill percentage and infill pattern for PLA (c) Effect of infill percentage for PMMA (d) Interaction of infill percentage and infill pattern for PMMA

Fig. 11. Compressive strength for both experiments. (a) Compressive strength for grid infill (b) Compressive strength for line infill

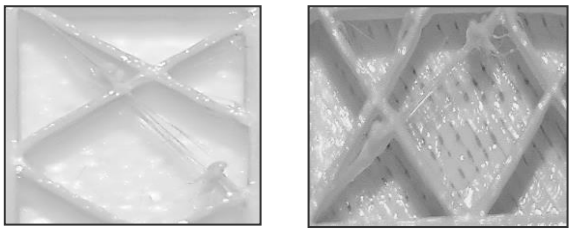

(a) (b)

Fig. 12. 10% of infill. (a) Line pattern (b) Grid pattern

4. FINDINGS

By comparing all the samples, it was observed that higher infill percentages provide strong compressive strength compared to lower infill percentages. This factor need to be emphasized in fabricating porous structures for determining compressive strength.The grid infill pattern yielded denser structure compared to the line infill pattern, as shown in Figure 13.

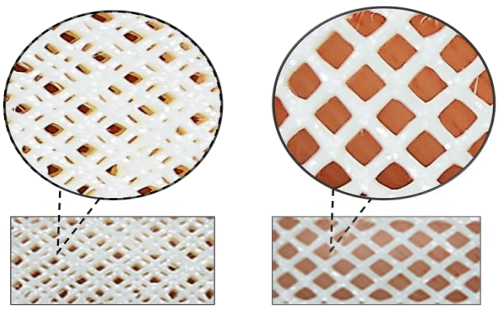

(a (b

Fig. 13. Comparison of scaffold structures. (a) Dense line layers (b) Less dense grid structure

A dense structure is not ideal for cell growth, in terms of porosity. These results show that the porosity and mechanical properties must be controlled to achieve the ideal conditions for cell growth.

The parameters can be manipulated to tailor the desired structure.The infill percentage significantly influences the porosity and mechanical properties of the structure, and the infill pattern must also be chosen for an optimum outcome. However, to successfully fabricate the desired structure, the design of the nozzle strongly affects the stability, consistency, and accuracy of the finished product. The specific design features of our nozzle contribute to the consistency and accuracy of printed structures, which also has an effect on the porosity and mechanical properties. The die angle is chosen specifically for the material to encourage stability in the extrusion process. The temperature inside the liquefier also needs to be addressed, as consistent temperature control is crucial. Our nozzle is adjustable enough to maintain the optimum temperatures for extruding biomaterials, which are 190°C for PLA and 200°C for PMMA. The structure in Figure 14 pictured with a scanning electron microscope (Hitachi SU1510, Japan) at ×55 times magnification shows the consistency of the structure in each layer,which determines the success of the scaffold fabrication.

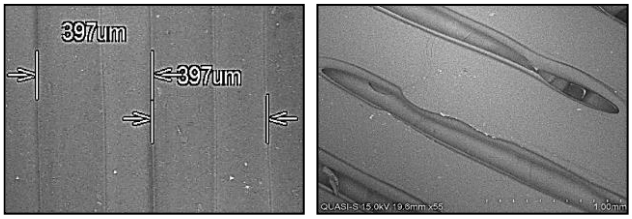

Fig. 14. Scanning Electron Microscopy image (×55 magnification). (a) Consistent layers of a finished part (b) One layer of a finished part

To demonstrate the fabrication of artificial bones for replacement surgeries, a model of the humerus bone was fabricated out of both PMMA and PLA with controlled porosities with a ratio of 1:0.7, as shown in Figures 15–17.

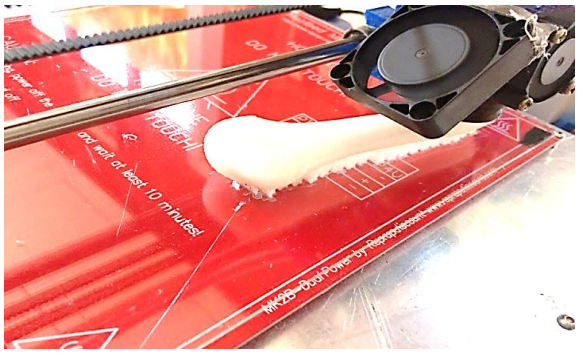

Fig. 15. Printing process using PMMA material with controlled porosities at ratio 1:0.7

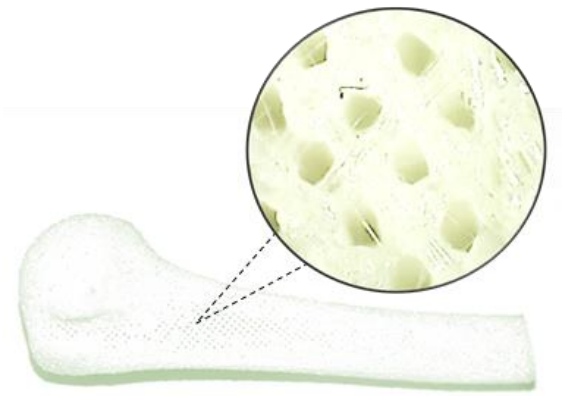

Fig. 16. Porous structure of the humerus bone model printed with PMMA (top)

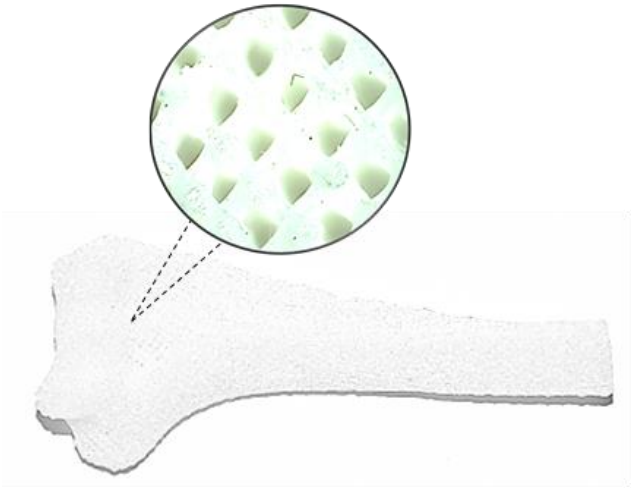

Fig. 17. Porous structure of the humerus bone model printed with PLA (bottom)

5. CONCLUSIONS

Biomedical scaffold structures were successfully fabricated using a novel 3D printer extruder nozzle, with the die angle, liquefier design, insulator, and tip diameter customised for biomedical polymers. The nozzle is capable of fabricating consistent and accurate scaffold structures by allowing us to manipulate the process parameters of infill percentage and infill pattern. Infill percentage and infill patterns significantly affect the porosity of a scaffold intended for cell growth.Our open-source 3D printer with a custom, new open-source, nozzle is capable of fabricating a scaffold structure with compressive strength between 12MPa and 20MPa and porosities between 50% and 70% accurately and consistently. These qualities provide the ideal conditions for cell growth; therefore, the nozzle can be used to print biomedical structures reliably, inexpensively, and simply. Some limitations on the finished product persist, even though the porosities and the mechanical properties achieve suitable conditions for cell growth. Further investigation is necessary, especially, intesting the samples for cell proliferation and observing cell growth. The

developed nozzle has proved to improve the consistency and accuracy of 3D prints; however, to achieve the desired low-cost biomedical rapid replicator, all systems of the open-source 3D printer must be taken into account. This involves choosing particular process parameters, which will differ for each machine. The movement of all axes that determines the accuracy of every movement for x, y, and z direction needs to be soundly constructed because it also affects the accuracy of the finished product. Overall, the modified nozzle provides a case study of how to modify low-cost 3D printer components for fabricating bone replacements.

6. REFERENCES

1. Bellini, A., Guceri, S., (2003). *Mechanical characterization of parts fabricated using fused deposition modeling*. Rapid Prototyp. J., **9**, pp. 252–264. https://doi.org/Doi 10.1108/13552540310489631.
2. Binnaz Hazar Yoruc, A., Cem Sener, B., (2015). *Biomaterials, in: A Roadmap of Biomedical Engineers and Milestones*. InTech. https://doi.org/10.1017/CBO9781107415324.004.
3. Brooks, H.L., Rennie, A.E.W., Abram, T.N., McGovern, J., Caron, F., (2012). *Variable Fused Deposition Modelling - Analysis of benefits, concept design and tool path generation*. Innov. Dev. Virtual Phys. Prototyp. - Proc. 5th Int. Conf. Adv. Res. Rapid Prototyp., pp. 511–517.
4. Chen, A. a, Tsang, V.L., Albrecht, D.R., Bhatia, S.N., (2007). *3-D Fabrication Technology for Tissue Engineering*. BioMEMS Biomed. Nanotechnology, III, Ther. Micro/Nanotechnology, pp. 23–38.
5. Espalin, D., Arcaute, K., Rodriguez, D., Medina, F., Posner, M., Wicker, R., (2010a). *Fused deposition modeling of patient-specific polymethylmethacrylate implants*. Rapid Prototyp. J., **16**, pp. 164–173, https://doi.org/10.1108/13552541011034825.
6. Espalin, D., Arcaute, K., Rodriguez, D., Medina, F., Posner, M., Wicker, R., (2010b). *Fused deposition modeling of patient-specific polymethylmethacrylate implants*. Rapid Prototyp. J., **16**, 164–173, https://doi.org/10.1108/13552541011034825.
7. Hutmacher, D.W., (2000). *Scaffolds in tissue engineering bone and cartilage*. Biomaterials **21**, pp. 2529–2543, https://doi.org/10.1016/S0142-9612(00)00121-6.
8. Jones, R., Haufe, P., Sells, E., Iravani, P., Olliver, V., Palmer, C., Bowyer, A., (2011). *RepRap – the replicating rapid prototype*, Robotica, **29**, 177–191. https://doi.org/10.1017/S026357471000069X.
9. Kalita, S.J., Bose, S., Hosick, H.L., Bandyopadhyay, A., (2003). *Development of controlled porosity polymer-ceramic composite scaffolds via fused deposition modeling*, Mater. Sci. Eng. C, **23**, 611–620. https://doi.org/10.1016/S0928-4931 (03)00052-3.
10. Liang, J.-Z., (1995). *Effect of the die angle on the extrusion swell of rubber compound*. J. Mater. Process. Technol., **52**, 207–212. https://doi.org/10.1016/0924-0136(94)01610-D.
11. Liang, J.Z., Ness, J.N., (1997). *Effect of die angle on flow behaviour for high impact polystyrene melt*. Polym. Test., **16**, 403–412.
12. Lutolf, M.P., Hubbell, J. a, (2005). *Synthetic biomaterials as instructive extracellular microenvironments for morphogenesis in tissue engineering*. Nat. Biotechnol., **23**, 47–55. https://doi.org/10.1038/nbt1055.
13. Melenka, G.W., Schofield, J.S., Dawson, M.R., Carey, J.P., (2015). *Evaluation of dimensional accuracy and material properties of the MakerBot 3D desktop printer*. Rapid Prototyp. J., **21**, 618–627, https://doi.org/10.1108/RPJ-09-2013-0093.
14. Monmaturapoj, N., Yatongchai, C., (2011). *Influence of preparation method on hydroxyapatite porous scaffolds*, **34**, 1733–1737.
15. Mostafa, N., Syed, H.M., Igor, S., Andrew, G., (2009). *A Study of Melt Flow Analysis of an ABS-Iron Composite in Fused Deposition Modelling Process*. Tsinghua Sci. Technol., **14**, 29–37. https://doi.org/10.1016/S1007-0214(09)70063-X.
16. Nair, L.S., Laurencin, C.T., (2006). *Polymers as Biomaterials for Tissue Engineering and Controlled Drug Delivery*. Adv. Biochem. Eng. / Biotechnol. **252**. https://doi.org/10.1007/11579328.
17. Onwubolu, G.C., Rayegani, F., (2014). *Characterization and Optimization of Mechanical Properties of ABS Parts Manufactured by the Fused Deposition Modelling Process*., Int. J. Manuf. Eng., 2014, **13**. https://doi.org/10.1155/2014/598531.
18. Park, S.H., Park, D.S., Shin, J.W., Kang, Y.G., Kim, H.K., Yoon, T.R., Shin, J.W., (2012). *Scaffolds for bone tissue engineering fabricated from two different materials by the rapid prototyping technique: PCL versus PLGA*. J. Mater. Sci. Mater. Med. **23**, 2671–2678. https://doi.org/10.1007/s10856-012-4738-8.
19. Ramanath, H.S., Chua, C.K., Leong, K.F., Shah, K.D., (2008). *Melt flow behaviour of poly-ε-caprolactone in fused deposition modelling*. J. Mater. Sci. Mater. Med. **19**, 2541–2550, https://doi.org/10.1007/s10856-007-3203-6.
20. Richardson, M., (2012). *Designer/Maker: The Rise of Additive Manufacturing*, Domestic-Scale Production and the Possible Implications for the Automotive Industry. Comput. Aided. Des. Appl. PACE, pp. 33–48, https://doi.org/10.3722/cadaps.2012.PACE.33-48.
21. Scalera, F., Gervaso, F., Sanosh, K.P., Sannino, A., Licciulli, A., (2013). *Influence of the calcination temperature on morphological and mechanical properties of highly porous hydroxyapatite*

scaffolds. Ceram. Int. **39**, 4839–4846. https://doi.org/10.1016/j.ceramint.2012.11.076.
22. Shor, L., Yildirim, E.D., Güçeri, S., Sun, W., (2010). *Printed Biomaterials*, 91–110. https://doi.org/10.1007/978-1-4419-1395-1.
23. Sukindar, N.A., Ariffin, M.K.A., Hang Tuah Baharudin, B.T., Jaafar, C.N.A., Ismail, M.I.S., (2016). *Analyzing the effect of nozzle diameter in fused deposition modeling for extruding polylactic acid using open source 3D printing*. J. Teknol. **78**. https://doi.org/10.11113/jt.v78.6265.
24. Sukindar, N.A., Khairol, M., Mohd, A., (2016). *An Analysis on Finding the Optimum Die Angle of Polylactic Acid* in Fused Deposition Modelling **835**, pp. 254–259, https://doi.org/10.4028/www.scientific.net/ AMM.835.254.
25. Zein, I., Hutmacher, D.W., Tan, K.C., Teoh, S.H., (2002). *Fused deposition modeling of novel scaffold architectures for tissue engineering applications*. Biomaterials **23**, 1169–1185, https://doi.org/10.1016/S0142-9612(01)00232-0.

Received: March 15, 2019 / Accepted: December 20, 2019 / Paper available online: December 25, 2019